CRYSTAL GROWTH & DESIGN

Article

Cite This: Cryst. Growth Des. 2017, 17, 5927-5934

pubs.acs.org/crystal

Phase Evolution of VO_2 Polymorphs during Hydrothermal Treatment in the Presence of AOT

Li Zhong,[†,‡] Kaibin Li,[†,‡] Yuanyuan Luo,[†] Ming Li,[†] Hua Wang,[†,‡] and Guanghai Li*[,†,‡]

[†]Key Laboratory of Material Physics, Anhui Key Laboratory of Nanomaterials and Nanotechnology, Institute of Solid State Physics, Chinese Academy of Sciences, Hefei 230031, P. R. China

[‡]University of Science and Technology of China, Hefei 230026, P. R. China

Supporting Information

ABSTRACT: VO_2 polymorphic nanoparticles (NPs) were synthesized by hydrothermal reaction in the presence of surfactant bis(2-ethylhexyl) sulfosuccinate sodium salt (AOT). The AOT acts as both growth inhibitor and soft template in the formation of VO_2 polymorphs, and there is a definite phase evolution process with prolonging reaction time: $(NH_4)_2V_6O_{16}\cdot 1.5H_2O \rightarrow NH_4V_4O_{10} \rightarrow VO_2(B) \rightarrow VO_2(B+D) \rightarrow VO_2(D) \rightarrow VO_2(D+P) \rightarrow VO_2(P)$. The formation mechanisms of the $VO_2(D)$ and $VO_2(P)$ phases were found to be, respectively, a dissolution−recrystallization and recrystallization process. The as-prepared $VO_2(P)$ can be easily transformed to $VO_2(M)$ NPs after a mild annealing treatment, and the $VO_2(M)$ composite films show an excellent infrared performances. The clarification of phase evolution of VO_2 polymorphs during hydrothermal treatment can help in understanding the formation mechanism and selective synthesis of different VO_2 metastable phases.

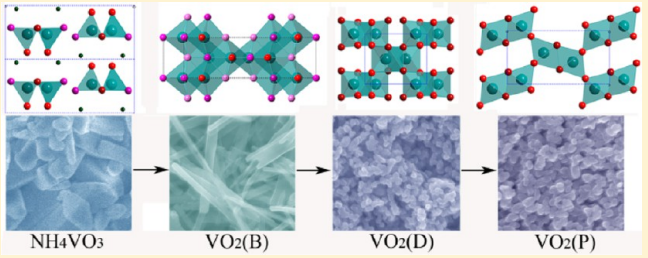

INTRODUCTION

Vanadium dioxide (VO_2) has numerous polymorphs, such as $VO_2(R)$, $VO_2(M)$, $VO_2(A)$, $VO_2(B)$, $VO_2(C)$,[1] $VO_2(D)$,[2] and $VO_2(P)$.[3,4] Among these polymorphs, the $VO_2(M)$ is widely studied in the past decades due to the reversible semiconductor−metal phase transition between $VO_2(M)$ and $VO_2(R)$ at a temperature of about 68 °C, accompanied by an abrupt change in optical and electrical performances, making it an attractive candidate for the wide use in energy saving and conservation fields.[5] Meanwhile, the $VO_2(B)$ is suitable for application in lithium ion batteries due to its proper electrode potential and layered structure.[6,7] Other metastable phases, such as $VO_2(D)$ and $VO_2(P)$, have been attracting increased interest due to their easy transformation to $VO_2(M)$.[3,8]

Many methods have been explored to fabricate $VO_2(M)$ NPs, such as solid-state reactions,[9,10] hydrothermal synthesis,[11−14] pulsed laser deposition,[15,16] and combustion route,[17,18] in which the hydrothermal synthesis combined with subsequently mild annealing treatment is an effective method,[3,8,19−21] due to its easy controlling of phase structure, morphology, and size of the NPs.[22,23] Recent studies found that the synthesis of the metastable $VO_2(D)$ or $VO_2(P)$ phase rather than the $VO_2(B)$ or $VO_2(A)$ phase will benefit the preparation of $VO_2(M)$ NPs because of their highly structural similarity with $VO_2(R)$ phase.[3,20,24,25]

Different phase evolution processes among VO_2 polymorphs have been proposed from metastable VO_2 polymorphs like $VO_2(D)$,[8] $VO_2(A)$,[25] $VO_2(P)$,[3,25] and $VO_2(B)$[24] to stable phase $VO_2(R/M)$. It was found that the $VO_2(M)$ nanorods can be formed from the nucleation of nanobumps on the surface of the $VO_2(B)$ nanorods, and an intermediate phase $VO_2\cdot xH_2O$ was first formed from the $VO_2(B)$, and then transformed to the $VO_2(A)$ nanobelts.[25] We found an evolution processes between V_2O_5 and $VO_2(M)$ by the sequence: $V_2O_5 \rightarrow V_3O_7\cdot H_2O \rightarrow VO_2(B) \rightarrow VO_2(A) \rightarrow VO_2(M)$ with increasing either reaction time or reaction temperature, and the oriented attachment (OA) mechanism is responsible for the formation of the $VO_2(M)$ nanorods.[26] A metastable $VO_2(A)$ was first formed, and then the $VO_2(M)$ by Ostwald mechanism forms $VO_2(B)$ to $VO_2(M)$.[27] The $VO_2(D)$ NPs can be formed by either self-assembly or Ostwald ripening of $VO_2(B)$ nanomaterials.[2,20,22] Doping can promote the phase evolution from metastable $VO_2(A_H)$ to $VO_2(M)$ by changing the atomic arrangement to form a similar structure to $VO_2(R/M)$.[12] Nevertheless, there is no report on the phase evolution between metastable $VO_2(D)$ and $VO_2(P)$. The reported formation mechanism of $VO_2(M)$ and the phase evolution process among VO_2 polymorphs depend strongly on the experimental conditions and reaction systems, and thus the understanding of the phase evolution process of VO_2 polymorphs is essential in the synthesis of the VO_2 with specific phase structure.

In this work, we report a controllable hydrothermal synthesis of VO_2 polymorphic NPs from ammonium metavanadate (NH_4VO_3) with the aid of surfactant bis(2-ethylhexyl)

Received: July 25, 2017
Revised: September 14, 2017
Published: October 11, 2017

DOI: 10.1021/acs.cgd.7b01037
Cryst. Growth Des. 2017, 17, 5927−5934

sulfosuccinate sodium salt (AOT). The VO_2 polymorphs like VO_2(B), VO_2(D), and VO_2(P) can be selectively synthesized by controlling hydrothermal parameters. The phase evolution among VO_2 polymorphs during hydrothermal reaction was analyzed and discussed, and the formation mechanisms of VO_2(P) and VO_2(D) phases were proposed. A mild annealing treatment was used to transform VO_2(P) to VO_2(M) NPs, and the infrared performance of VO_2(M) composite films was investigated.

EXPERIMENTAL SECTION

Materials. All chemicals were used without further purification after purchase. Ammonium metavanadate (NH_4VO_3) was purchased from the Research Institute of Tianjin Guangfu Fine Chemical Research Institute. Formic acid (HCOOH), alcohol (AR), and polyvinylpyrrolidone (PVP-K30) were from Chinese Sinopharm Chemical Reagent Co., Ltd. AOT was from TCI (Shanghai) Development Co., Ltd.

Synthesis. For a typical synthesis, 0.2338 g of NH_4VO_3 and 0.1 g of AOT were first dissolved into 20 mL of deionized water with continued magnetic stirring for 2 h; then, formic acid (88 wt %, 0.9 mL) was added drop by drop into the light yellow solution with magnetic stirring for another 5−10 min. Then, the precursor solution was sealed in a 40 mL Teflon cup and placed in a sealed autoclave for hydrothermal treatment at 220 °C for 2 days in an oven. After cooling down to room temperature naturally, the precipitate was dried at 60 °C in air after cleaning with hot water (~60 °C) and alcohol alternatively. The as-prepared product was finally annealed at 250−350 °C for 1.5 h in a vacuum furnace to obtain VO_2(M) NPs.

Characterizations. The size, morphology, and crystal structure of the products were characterized by X-ray power diffractometer with a Cu Kα line (XRD, PANalytical X'Pert), field-emission scanning electronic microscope (FESEM, Hitachi SU8020), and high resolution transmission electronic microscope (HRTEM, JEOL JEM-2010). The phase transition temperature was analyzed by a differential scanning calorimeter (DSC, PerkinElmer Pyris Diamond) at a heating rate of 10 °C/min in a flowing nitrogen atmosphere. The optical transmission spectra of VO_2(M) NPs composite films were recorded by a UV/vis/NIR spectrophotometer (Shimadzu UV3600-MPC3100) at the wavelength of 300−2400 nm equipped with a temperature controller.

RESULTS AND DISCUSSION

3.1. Synthesis of VO_2(P) NPs. Figure 1 shows an XRD pattern of the product (AOT content: 0.1 g) washed with alcohol and hot water (~60 °C) alternately. All the XRD diffraction peaks can be well indexed to VO_2(P) (JCPDS card no. 73-0514), indicating the formation of pure VO_2(P) phase.

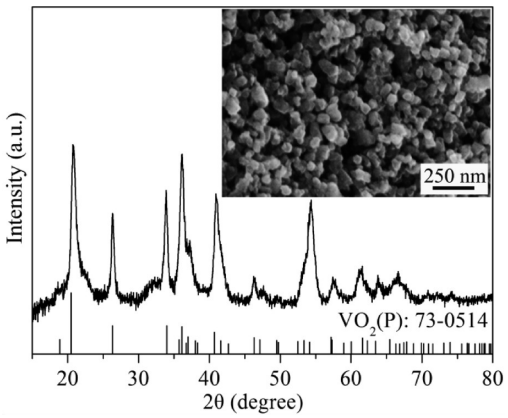

Figure 1. XRD pattern of VO_2(P) NPs; the inset is the corresponding FESEM image.

The inset in Figure 1 shows a typical FESEM image of the product. One can see that the VO_2(P) is composed of quasi-sphere NPs with an average size of about 89 nm. It was found that washing with hot water is essential in obtaining pure VO_2(P) NPs, and a phase mixture of VO_2(P) NPs and NH_4VO_3 nanosheets was obtained if washing with only alcohol (Figure S1 of the SI). Washing with alcohol can only remove the residual organic in the original precipitate, such as AOT, rather than NH_4VO_3, while washing with hot water can remove the residual NH_4VO_3 because of its high solubility in hot water.

3.2. Phase Evolution of VO_2 Polymorph. *The Influence of AOT.* In the surfactant-assisted hydrothermal reaction, the surfactant has a significant influence on the morphology and crystal structure of the product. Different surfactants have been used to fabricate VO_2, such as cetyltrimethylammonium bromide.[28] polyvinylpyrrolidone,[29] sodium dodecyl sulfate,[30] and polyethylene glycol.[31] The surfactant not only provides a microenvironment for the growth of vanadium oxide nanomaterials but also plays a template role for directing the formation of nanomaterials.[32] We found the surfactant AOT content has a great influence on the phase structure and phase evolution of VO_2. In the following discussions, all the hydrothermal reactions are performed at 220 °C for 48 h, and the products were washed with only alcohol. Figure 2 shows FESEM images

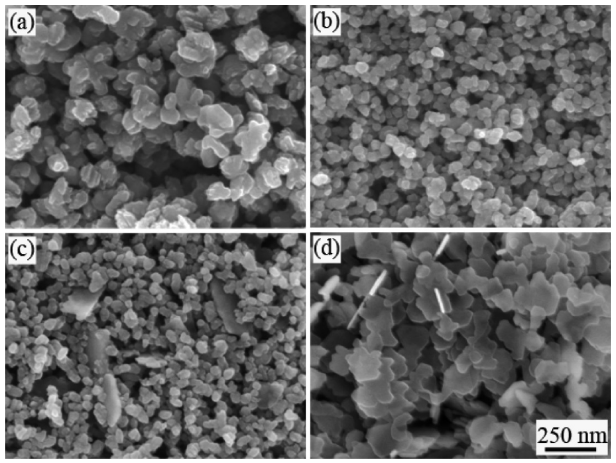

Figure 2. FESEM images of products with AOT content of (a) 0.01, (b) 0.05, (c) 0.10, and (d) 0.50 g.

of the products obtained with different AOT contents. One can see the product is composed of quasi-sphere NPs and nanorods with irregular branches with an AOT content of 0.01 g, as shown in Figure 2a. When the AOT content was increased to 0.05 g, the product is quasi-sphere NPs with a nearly uniform size distribution; see Figure 2b. A small number of nanosheets appear together with the quasi-sphere NPs when the AOT content was increased to 0.1 g; see Figure 2c. Almost pure nanosheets were obtained with the AOT content of 0.5 g; see Figure 2d.

Figure 3 shows the XRD patterns of the products with different AOT contents, and the corresponding TEM and HRTEM characterizations are shown in Figure 4. Table S1 summarizes the influence of AOT content on the corresponding products. One can see a phase mixture of VO_2(D) and VO_2(P) is formed with 0.01 g of AOT; see curve (1) in Figure 3. The corresponding SAED pattern of the circle area of a branched nanorod in Figure 4a can be well indexed to VO_2(D) (the crystallographic plane indices are indexed according to

DOI: 10.1021/acs.cgd.7b01037
Cryst. Growth Des. 2017, 17, 5927−5934

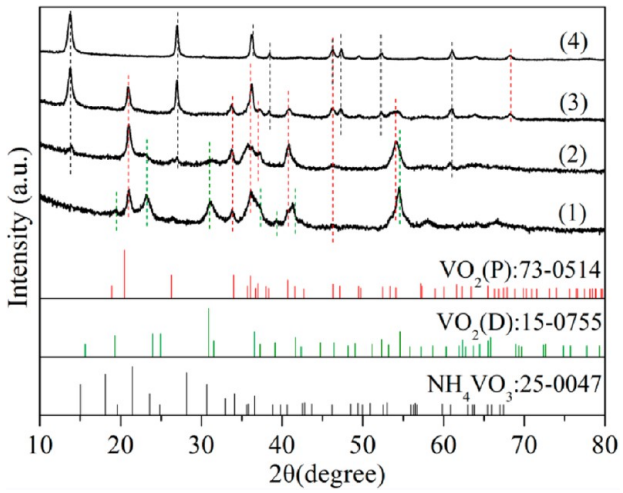

Figure 3. XRD patterns of product with AOT content of (1) 0.01, (2) 0.05, (3) 0.1, and (4) 0.5 g.

Xie's report[33]), indicating that the branched nanorods are VO_2(D) phase. For 0.05 g AOT content, the product consists of mainly VO_2(P) NPs with less VO_2(D) and NH_4VO_3 phases, as proved by curve (2) in Figure 3, in which the intensities of the diffraction peaks from the VO_2(D) and NH_4VO_3 phases become very weak. The corresponding TEM analysis shown in Figure 4b proves that the NPs with a quasi-spherical shape are VO_2(P), in which the interplanar distances of 0.183, 0.185, and 0.265 nm match well with the (230), ($\bar{1}$31), and (101) planes of VO_2(P) phase, as shown by the SAED pattern of the circle area in the right inset of Figure 4b. With 0.1 g of AOT, the product is a phase mixture of VO_2(P) NPs and NH_4VO_3 nanosheets (Figure 4c), and the NH_4VO_3 content is higher than that with 0.05 g of AOT because of the enhanced intensities of the XRD diffraction peaks, as shown in curves (2) and (3) of Figure 3. The NH_4VO_3 nanosheets become dominant with 0.5 g of AOT, as shown in curve (4) of Figure 3.

From the above results, one can clearly see the addition of AOT surfactant will change not only the morphology but also the phase structure of the products. The surfactant can be a growth inhibitor or a soft template in a hydrothermal reactant system.[28,34] Without AOT, the product is composed of the star-shaped VO_2(D) NPs and VO_2(B) nanorods (see Figure S2 of the SI), as has been reported in our previous study, in which the reconstruction of VO_2(B) leads to the formation of VO_2(D).[20] With addition of 0.01 g of AOT, the star-shaped VO_2(D) NPs becomes irregular nanorods, and the VO_2(P) NPs were formed instead of the VO_2(B) nanorods. AOT can reduce the surface tension of the solution in the hydrothermal reaction system, and thereby reduce the energy needed to form a new phase in the solution.[33] In the beginning of hydrothermal reaction, AOT will partly cover the surface of not only NH_4VO_3 raw material but also the newly formed VO_2(B) nucleuses; in the latter case, the AOT will not affect the growth of the VO_2(B) nanorods, but reduce the energy needed for the formation of VO_2(D), leading to the transformation from VO_2(B) to VO_2(D) nanorods with regular branches. With only 0.01 g, the coverage of the AOT on the VO_2(D) nanorods is incomplete because of very low content, resulting in the formation of the VO_2(P) nanobumps on the surface of the VO_2(D) nanorods, as proved from the below discussion of the formation of the irregular branches of the VO_2(D) nanorods. With increasing the AOT content from 0.01 to 0.05 g, all the surface of the VO_2(D) nucleuses will be covered by AOT, and an anisotropic growth of the VO_2(D) nucleuses to form a star-

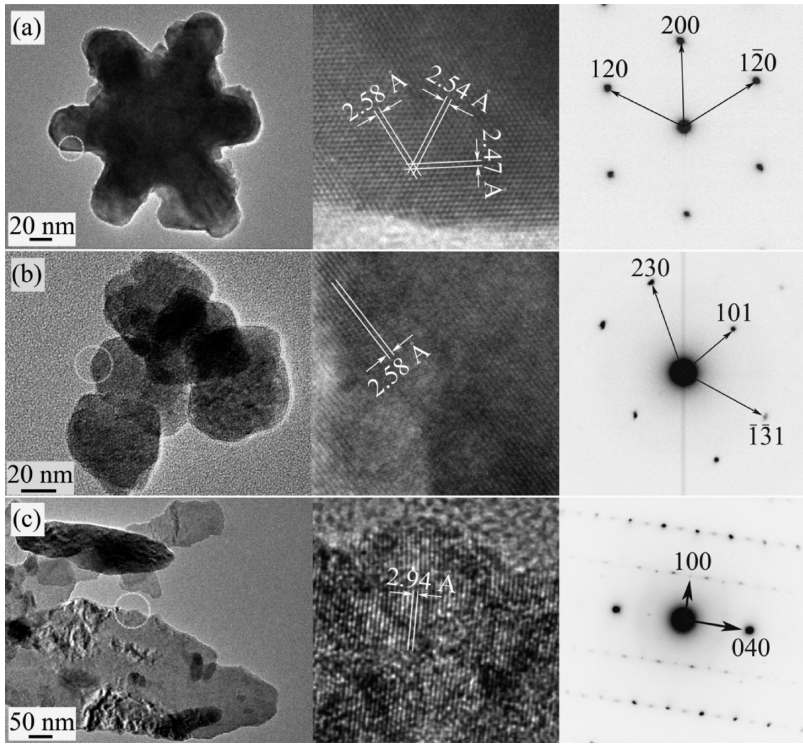

Figure 4. TEM images of products synthesized with AOT content of (a) 0.01, (b) 0.05, and (c) 0.1 g. The right insets are the corresponding HRTEM image and SAED pattern of the circle area.

DOI: 10.1021/acs.cgd.7b01037
Cryst. Growth Des. 2017, 17, 5927−5934

shaped morphology is restricted, leading to the formation of the VO_2(P) NPs. If the AOT addition content is too high, such as 0.5 g, the surface of the NH_4VO_3 raw material will be fully covered, and in this case, the AOT, on the one hand, will act as a soft template to induce a self-assembly of NH_4VO_3, leading to the formation of the NH_4VO_3 nanosheets, and, on the other hand, will restrict the reduction of NH_4VO_3 by formic acid, suppressing the formation of VO_2(D) as well as VO_2(P) phases. Besides AOT surfactant, the formic acid content and the reaction temperature and time also affect the morphology and phase structure of the products.

The Influence of Formic Acid. The XRD patterns and FESEM images of the products synthesized with different formic acid contents (with constant 0.05 g of AOT) are shown in Figures S3 and S4 of the SI, and the results are summarized in Table S1. One can see the lower the formic acid content, the lower the NH_4VO_3 nanosheets content, and no NH_4VO_3 was observed with 0.5, 0.3, and 0.1 mL of formic acid content. On the other hand, the higher the content of the formic acid, the higher the VO_2(P) NPs content, and the lower the formic acid content, the higher the VO_2(D) nanorods content. With 0.3 mL of formic acid, the product is pure VO_2(D) spindle nanorods, and with 0.1 mL of formic acid, the product is pure VO_2(D) phase with a chaotic configuration. The surface properties of metal oxides depend on the pH value of the reaction solution, and the surface charge density of the metal oxides will decrease with increasing pH value of the reaction solution because of the desorption of protons, leading to an increase in the interfacial free energy of the reaction system.[35] The formic acid will change the pH value of the reaction solution, thereby altering the charged state of the reagents, and thus affecting the coverage of the AOT on the reagents and resultants, leading to the formation of the products with different morphologies and phase structures.

The Influence of Temperature. The XRD patterns and FESEM images of products synthesized at different temperatures with 0.05 g of AOT and 0.9 mL of formic acid are shown in Figures S5 and S6 of the SI, and the results are summarized in Table S1. One can see a phase mixture of VO_2(D), VO_2(P), and NH_4VO_3 was obtained at the temperatures of 180, 200, and 220 °C. A low temperature of 180 °C is a benefit for the formation of the VO_2(D) NPs, and the VO_2(P) content increases with increasing temperature. A high temperature of 250 °C is a benefit for the formation of the VO_2(P) NPs with slight VO_2(D) NPs and without NH_4VO_3. It was found, with increasing reaction time at 250 °C with 0.1 g of AOT, the content of the VO_2(P) NPs increases, while that of the VO_2(D) NPs decreases, and almost pure VO_2(P) NPs were obtained for 2.5 days (Figure S7 of the SI). The product contains a large number of VO_2(P) NPs reacted at 250 °C even with 0.5 g of AOT, which is much different from the products obtained at 220 °C. The above results indicate that temperature plays as a crucial role in the formation of pure VO_2(P) NPs. High temperature will excite AOT molecules and the AOT/water system can turn to an isotropic liquid that will lead to the growth of crystalline by the natural habit of crystalline.[36] In this study, we speculate that a high temperature will restrain AOT from complete coverage on the NH_4VO_3 raw material, in which the role of the AOT as a soft template will be weaken, favoring the reduction of NH_4VO_3 by formic acid and coverage of the AOT on the VO_2 nucleuses, and thus the formation of the VO_2(P) phase.

3.3. Growth Mechanisms of VO_2(D) and VO_2(P) NPs.

To understand the growth mechanism of the VO_2(D) and VO_2(P) NPs and clarify the phase evolution of VO_2 polymorphs, a series of experiments were performed for different reaction times at 220 °C with 0.9 mL of formic acid, and products were washed with only alcohol. Figures 5 and 6 show the XRD patterns and FESEM images of products obtained at different reaction times with an AOT content of 0.01 g, and the results are summarized in Table S1. One can see $NH_4V_4O_{10}$ was formed after hydrothermal reaction for 2 h, and a massive VO_2(B) nanorod was formed when the reaction time increased to 4.5 h, in which some of the VO_2(B) nanorods start to dissolve to form VO_2(D) NPs. Increasing the reaction time to 7.5 h, pure star-shaped VO_2(D) NPs with regular branches and a smooth surface were formed. After reaction for 24 h, the diffraction peaks from the VO_2(P) phase appear, indicating the formation of the VO_2(P) NPs, and their intensity increases with increasing the reaction time from 24 to 34 h, and then to 48 h, demonstrating an increased content of the VO_2(P) NPs in the products. The corresponding FESEM images shown in Figure

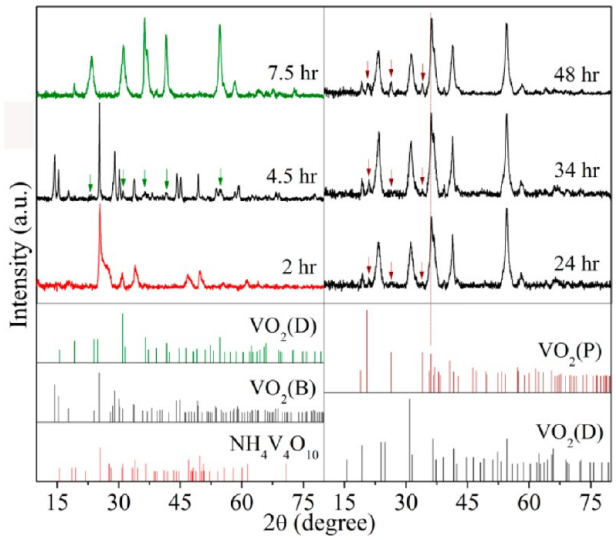

Figure 5. XRD patterns of products with different reaction times at 220 °C with 0.01 g of AOT and 0.9 mL of formic acid.

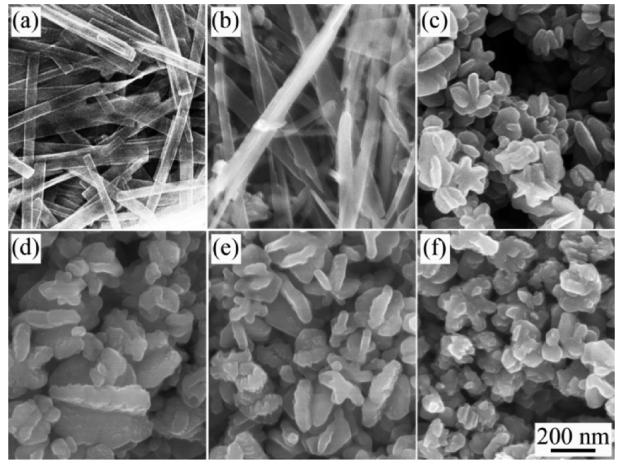

Figure 6. FESEM images of product with reaction time for (a) 2, (b) 4.5, (c) 7.5, (d) 24, (e) 34, and (f) 48 h at 220 °C with 0.01 g of AOT and 0.9 mL of formic acid.

DOI: 10.1021/acs.cgd.7b01037
Cryst. Growth Des. 2017, 17, 5927−5934

6c–f indicate that the longer the reaction time, the rougher the surface of the VO_2(D) nanorods and the higher the content of the nanobumps on the surface of the VO_2(D) nanorods. After reaction for 48 h, the VO_2(D) nanorods become irregular branches and the size of the nanobumps increases substantially. Since the nanorods are VO_2(D), the nanobumps must be VO_2(P) NPs. TEM observations clearly show the coexistence of the separated VO_2(D) and VO_2(P) NPs in the product synthesized at 250 °C for 36 h with 0.01 g of AOT (Figure S8), and no orientation relationships were found between VO_2(D) and VO_2(P) NPs. These results indicate that the VO_2(P) nanobumps will grow up and separate from VO_2(D) NPs (or nanorods), and from which we can arrive at the conclusion that the phase transition from VO_2(D) to VO_2(P) is a recrystallization process. Without AOT, the product was composed of the star-shaped VO_2(D) NPs and VO_2(B) nanorods even after reaction for 48 h, and with only 0.01 g of AOT, the star-shaped VO_2(D) NPs were formed after reaction for only 7.5 h, indicating that AOT indeed reduces the energy needed for the formation of VO_2(D), leading to a complete transformation from VO_2(B) to VO_2(D) nanorods. AOT also can promote the phase transition from VO_2(D) to VO_2(P), in which the VO_2(P) nanobumps can heterogeneously nucleate and grow on the surface of VO_2(D) because of part coverage of the AOT on the surface of VO_2(D), which is similar to the formation of VO_2(M) nanobumps on VO_2(B) nanorods.[37]

When the AOT content was increased to 0.05 g, and after hydrothermal reaction for 1 h, only a small number of $NH_4V_4O_{10}$ nanobelts were formed together with a large number of $(NH_4)_2V_6O_{16}\cdot1.5H_2O$ nanobelts, and the content of the $NH_4V_4O_{10}$ nanobelts increases with increasing the reaction time to 2 h. See Figure 7a,b, and Figure S9 of the SI, and the results are summarized in Table S1. The $NH_4V_4O_{10}$ nanobelts disappear and plenty of VO_2(B) nanorods form with a small number of VO_2(D) NPs when the reaction time increased to 2.5 h, and the content of the VO_2(D) NPs increases with increasing the reaction time to 3.5 h. FESEM and HRTEM characterizations prove that the formation of the VO_2(D) NPs is a dissolution–recrystallization process of the VO_2(B) nanorods, as shown Figure 7. The VO_2(B) nanorods are single crystalline and grow along the [001] direction, and the interplanar distances of 0.196, 0.259, and 0.192 nm of an NP on a VO_2(B) nanorod match well with (210), (020), and $(\bar{2}10)$ planes of VO_2(D) phase, indicating the formation of VO_2(D) phase; see Figure 7d,e. Figure 8 shows the XRD patterns of the products synthesized at reaction times longer than 3.5 h. One can see the VO_2(B) nanorods are totally dissolved and nearly pure VO_2(D) NPs are formed after reaction for 4.5 h, and the particle-like morphology can be clearly seen in Figure 9a. TEM analysis shown in Figure 9e confirms the formation of VO_2(D), in which the interplanar distances of 0.216, 0.215, 0.219, and 0.212 nm match well with (121), $(\bar{1}2\bar{1})$, $(2\bar{1}0)$, and (211) planes of VO_2(D) phase. With further prolonging the reaction time from 4.5 to 17, 24, 29, 41, and 48 h, the diffraction peaks gradually shift to low angle, and finally can be well indexed to VO_2(P) phase (JCPDS card no. 73-0514) after reaction for 48 h. From Figure 9a–d, one can see the VO_2(P) NPs have a sphere-like morphology, and their size increases with increasing reaction time, which is different from that of the VO_2(D) NPs, and further demonstrating the phase transition from VO_2(D) NPs to VO_2(P) NPs is a recrystallization process. The morphology of the VO_2(D) NPs

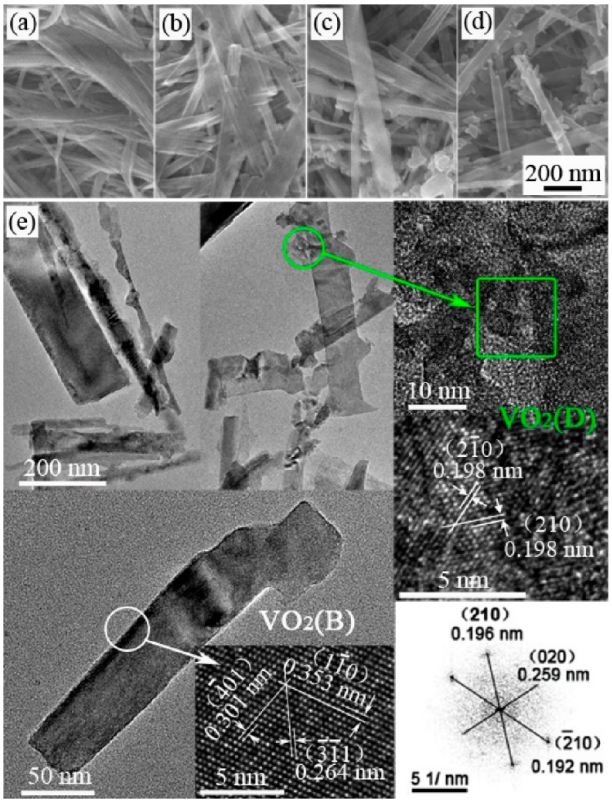

Figure 7. FESEM images of product with reaction time of (a) 1, (b) 2, (c) 2.5, and (d) 3.5 h at 220 °C with 0.05 g of AOT and 0.9 mL of formic acid. (e) TEM images of products with reaction time of 3.5 h. The insets in (e) are the HRTEM image and the corresponding SAED pattern of the circle area.

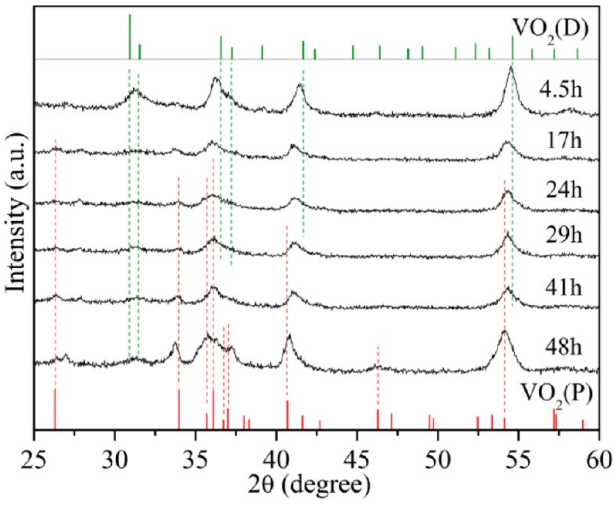

Figure 8. XRD patterns of product with reaction time for 4.5, 17, 24, 29, 41, and 48 h at 220 °C with 0.05 g of AOT and 0.9 mL of formic acid.

formed with 0.05 g of AOT is very different from that formed with 0.01 g of AOT, indicating the surface of the VO_2(D) nucleuses has been completely covered by AOT, and the anisotropic growth of VO_2(D) nucleuses to form a star-shaped morphology is restricted.

Under hydrothermal conditions, NH_4VO_3 particles (orthorhombic structure,[38] Figure S10) are initially reduced and fused into layered hydrated vanadium oxide intermediate compounds

DOI: 10.1021/acs.cgd.7b01037
Cryst. Growth Des. 2017, 17, 5927–5934

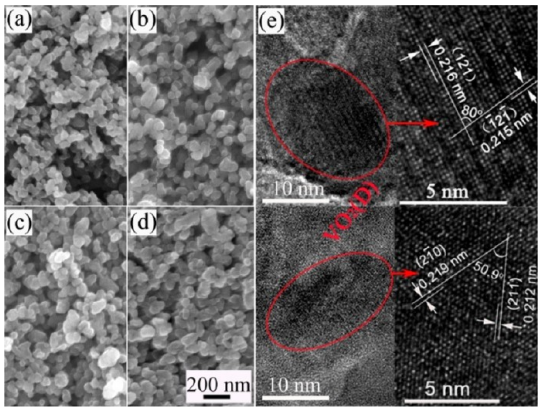

Figure 9. FESEM images of product with reaction time of (a) 4.5, (b) 17, (c) 24, and (d) 48 h at 220 °C with 0.05 g of AOT and 0.9 mL of formic acid. (e) TEM images of products with reaction time of 4.5 h. The insets in (e) are the HRTEM images of the circle area.

$(NH_4)_2V_6O_{16}\cdot 1.5H_2O$,[39] and then to another layer structure $NH_4V_4O_{10}$.[40] Further reduction results in reassembly into VO_2(B) nanorods. With prolonging time, the VO_2(B) gradually dissolved and recrystallized to form VO_2(D) NPs.[20] As time elapses further, the well-formed VO_2(D) structure is broken, and a phase transition from VO_2(D) to VO_2(P) happens. Among all the VO_2 polymorphs, the VO_2(B) phase (monoclinic structure,[41] Figure S10) is the least thermodynamically favorable phase with the lowest formation energy, while the VO_2(M) phase is the most thermodynamically favorable phase with the highest formation energy.[42] Other polymorphs like VO_2(D) (monoclinic structure,[33] Figure S10) and VO_2(P) (orthorhombic structure,[4] Figure S10) generally serve as the intermediate phases between VO_2(B) and VO_2(M). The phase transition between VO_2(B) and VO_2(D) or between VO_2(D) and VO_2(P) is a reconstructive one and cannot take place simply by slight movement of V^{4+} in VO_6 octahedral basic units like that between VO_2(P) and VO_2(R).[4] Our results clearly indicate that the AOT content and temperature have significant effects on the crystal growth and phase formation. The appearance of the VO_2(D) and VO_2(P) phases with increasing hydrothermal time and temperature could be understood from the perspective of thermodynamics/kinetics. There is the free energy and the internal energy difference between VO_2 polymorphs, partly owing to the different structural tension within the VO_2 crystal lattice.[27] The VO_2(B) phase can be readily transformed into VO_2(D) and then VO_2(P) phase with increasing hydrothermal time according to thermodynamic expectations. The AOT will not only affect the nucleation and crystal growth of VO_2 polymorphs when acted as a growth inhibitor or soft template but also change the structural tension of VO_2 polymorphs when absorbed on the surface of VO_2 crystals, and thus will affect the phase transitions of VO_2 polymorphs.

The above results demonstrate that there is a definite phase evolution process of $(NH_4)_2V_6O_{16}\cdot 1.5H_2O \rightarrow NH_4V_4O_{10} \rightarrow VO_2(B) \rightarrow VO_2(B+D) \rightarrow VO_2(D) \rightarrow VO_2(D+P) \rightarrow VO_2(P)$ with prolonging reaction time in the presence of AOT surfactant, and the synthesis of pure VO_2(B) nanorods, and VO_2(D) and VO_2(P) NPs can be realized simply by changing the hydrothermal parameters with the aid of AOT surfactant.

3.4. VO_2(M) NPs and Infrared Performance. Our results indicate that 0.05 and 0.1 g of AOT are the suitable addition contents for the synthesis of pure VO_2(P) NPs with an average size of about 59 and 89 nm, respectively, after alternately washing with hot water and alcohol, as shown in Figures S11 and S12 of the SI. Being having a similar crystal structure, the phase transition from VO_2(P) to VO_2(R) can take place with a mild annealing treatment. In the following discussion, the phase transition characters of the VO_2(M) NPs after annealing treatment of the VO_2(P) NPs at different temperatures were studied. The phase transition from VO_2(D) to VO_2(M) NPs can be found in our previous reports.[8,20]

Figure 10 shows the XRD patterns of the products after annealing of the VO_2(P) NPs at temperatures of 250, 300, and

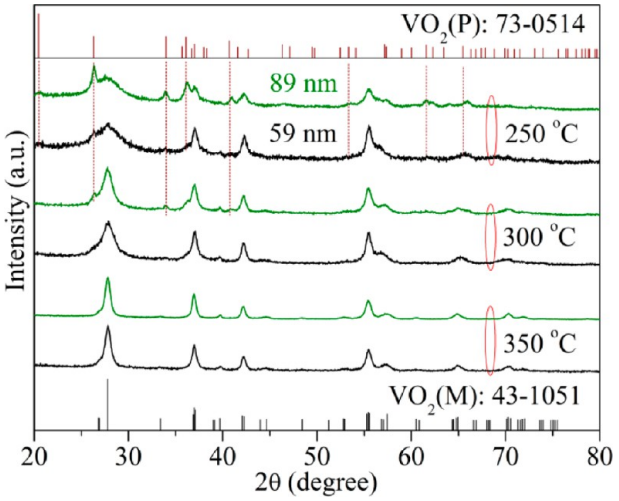

Figure 10. XRD patterns of VO_2(P) NPs after annealing treatment at different temperatures.

350 °C for 1.5 h in a vacuum. One can see the VO_2(P) NPs can partially transform to VO_2(M) NPs at 250 °C, and the content of the VO_2(M) NPs increases with increasing annealing temperature, and when annealed at 350 °C, pure VO_2(M) NPs were obtained, which is independent of the size of the VO_2(P) NPs. FESEM observations proved that no size and morphology changes occur after phase transformation from VO_2(P) to VO_2(M) NPs, which is in a good agreement with previous report.[3]

Figure 11 shows the DSC curves of the VO_2(M) NPs after annealing treatment of the VO_2(P) NPs at different temperatures. No phase transition can be observed for the VO_2(M) NPs obtained at 250 °C due to their weak crystallinity, while a reversible structural phase transition can be seen for the VO_2(M) NPs obtained at 300 and 350 °C. One also can see the phase transition temperature (T_c) from VO_2(M) to VO_2(R) (and vise visa) depends on grain size. For the VO_2(M) with the size of 59 nm, the T_c is about 55.9 and 70 °C during the heating cycle, and 39.3 and 53 °C during the cooling cycle, and the hysteresis width is about 16.6 and 17 °C for the VO_2(M) NPs obtained at 300 and 350 °C, respectively. With the VO_2(M) with the size of 89 nm, T_c is about 63.8 and 73.3 °C during heating, and 45.2 and 53.5 °C during the cooling cycle, and the hysteresis width is about 18.6 and 19.8 °C for the VO_2(M) NPs obtained at 300 and 350 °C, respectively. This result indicates that the VO_2(M) NPs with a smaller grain size have a lower T_c, whereas it was found in previous studies that the smaller the grain size, the higher the phase transition temperature for VO_2(M) nanocrystals.[43,44] The interfacial effect rather than the size effect is considered responsible for the DSC results shown

DOI: 10.1021/acs.cgd.7b01037
Cryst. Growth Des. 2017, 17, 5927−5934

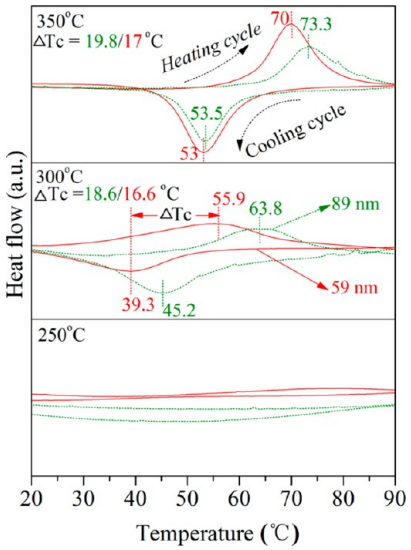

Figure 11. DSC curves of products with two sizes annealed for 1.5 h in a vacuum furnace at 250, 300, and 350 °C, respectively.

in Figure 11, as has been proved in previous studies.[3,8] The grain size of VO_2(M) NPs can be calculated from Scherrer's formula: where D is the mean size of grain size, K is a dimensionless shape factor with a typical value of about 0.89 for spherical particles, λ the X-ray wavelength, β the line broadening at half the maximum intensity after subtracting the instrumental line broadening, and θ the Bragg angle. The calculated results show that the grain size is about 18 nm for the 59 nm VO_2(M) NPs, while it is 23 nm for the 89 nm VO_2(M) NPs. Clearly, these VO_2(M) NPs are polycrystalline, and there are many grain boundaries. The corresponding TEM observations of the 89 nm VO_2(M) NPs also proved that the VO_2(M) NPs are polycrystalline, in which the NPs consisting of several small grains marked by the circles can be clearly seen, and the grain size slightly larger than that calculated by the Scherrer's formula, as shown in Figure S13. A smaller NP will have a higher density of surface defects, and the grain boundaries will act as nucleation sites for the phase transition between VO_2(M) and VO_2(R),[3,8] which will reduce the phase transition temperature of VO_2(M) NPs.

For practical application in smart windows, a composite film with VO_2(M) NPs dispersed in a dielectric matrix is of great advantages.[45] The VO_2(M) NPs with an average size of 59 nm were used to fabricate the composite films. 5 wt % VO_2(M) NPs and 5 wt % PVP were ball-milled in alcohol to get the dispersion solution. By changing the spin rate and the repeated times on the glass substrate, four composite films with different thicknesses were prepared. Figure S14 of the SI shows the optical transmittance of the VO_2(M) composite films before (25 °C) and after (100 °C) phase transition. One can see the VO_2(M) composite films demonstrate a thickness-dependent optical transmittance in both visible light and infrared regions. Also, the thicker the composite film, the higher the infrared modulation, and the lower the visible light transmittance. The integrated luminous (T_{lum}) and solar irradiation transmittances (T_{sol}) of the films, calculated from a previously reported method,[20] are shown in Table S2 of the SI. One can see the solar modulation ability (ΔT_{sol}) will be improved by increasing the thickness of the composite film at the cost of visible light transmittance. Even for the thinnest composite film, the infrared modulation is about 9.7% with a visible light transmittance as high as 53.4%, indicating the practicability of the composite film acting as smart windows. The VO_2(M) composite film with a thickness of 232 nm shows a comparable infrared modulation ability (12.7%) to that of the continuous thin film (12.99%),[46] and the optimized five-layered TiO_2/VO_2/TiO_2/VO_2/TiO_2 film (12.1%),[47] with an increased visible light transmittance of about 15.6% and 2.5%, respectively.

CONCLUSION

In summary, VO_2(B), VO_2(D), and VO_2(P) polymorphic NPs have been selectively synthesized by one-step hydrothermal reaction with the aid of AOT surfactant. The AOT acts as both growth inhibitor and soft template in the formation and phase evolution of VO_2 polymorphs. Different phase evolution processes have been observed depending on the content of AOT and formic acid as well as hydrothermal reaction temperature and time. A distinct time-dependent phase evolution has been demonstrated, in which VO_2(B) nanorods first nucleated and grew in size, then gradually dissolved and recrystallized to form VO_2(D) NPs based on a dissolution−recrystallization growth mechanism; because of coverage of AOT, further growth of VO_2(D) NPs is not allowed, and finally a phase transition from VO_2(D) to VO_2(P) happens via a recrystallization process. The VO_2(P) NPs can be easily transformed to VO_2(M) NPs by subsequently mild annealing treatment without noticeable changes in both morphology and size, and the resultant VO_2(M) composite films show excellent infrared performance. Our work demonstrates a good example of a controllable synthesis of VO_2 polymorphs with the aid of AOT surfactant, and will help in understanding the formation mechanism and selective synthesis of different VO_2 metastable phases.

ASSOCIATED CONTENT

Supporting Information

The Supporting Information is available free of charge on the ACS Publications website at DOI: 10.1021/acs.cgd.7b01037.

XRD pattern and FESEM image of the product washed with only alcohol; XRD pattern and FESEM image of the product synthesized without AOT; XRD patterns and FESEM images of the products synthesized with different formic acid contents; XRD patterns and FESEM images of the products synthesized at different temperatures and times with 0.05 g of AOT and 0.9 mL of formic acid; FESEM, TEM, HRTEM images of the product synthesized at 250 °C with 0.01 g of AOT; XRD patterns of the products synthesized at 220 °C for different times with 0.05 g of AOT and 0.9 mL of formic acid; crystal structures of NH_4VO_3, VO_2(B), VO_2(D), and VO_2(P) viewed along c-axes; XRD patterns, FESEM images, and size distribution histograms of the products washed with hot water and alcohol with AOT contents of 0.05 and 0.1 g; TEM images of 89 nm VO_2(M) NPs; optical transmittance spectra of the VO_2(M) composite films with different thicknesses by spin-coating VO_2(M) NPs dispersion solution; integrated luminous (T_{lum}) and solar irradiation transmittance (T_{sol}) of the VO_2(M) composite films (PDF)

AUTHOR INFORMATION

Corresponding Author

*E-mail: ghli@issp.ac.cn.

DOI: 10.1021/acs.cgd.7b01037
Cryst. Growth Des. 2017, 17, 5927−5934

ORCID

Guanghai Li: 0000-0002-1593-5584

Notes

The authors declare no competing financial interest.

■ ACKNOWLEDGMENTS

This work was financially supported by the National Natural Science Foundation of China (Grants 51372250, 51402304, and 51471163).

■ REFERENCES

(1) Zhang, L. M.; Xia, F.; Song, Z. D.; Webster, N. A. S.; Luo, H. J.; Gao, Y. F. *RSC Adv.* **2015**, *5*, 61371−61379.
(2) Song, Z. D.; Zhang, L. M.; Xia, F.; Webster, N. A. S.; Song, J. C.; Liu, B.; Luo, H. J.; Gao, Y. F. *Inorg. Chem. Front.* **2016**, *3*, 1035−1042.
(3) Sun, Y. F.; Jiang, S. S.; Bi, W. T.; Long, R.; Tan, X. G.; Wu, C. Z.; Wei, S. Q.; Xie, Y. *Nanoscale* **2011**, *3*, 4394−401.
(4) Wu, C. Z.; Hu, Z. P.; Wang, W.; Zhang, M.; Yang, J. L.; Xie, Y. *Chem. Commun.* **2008**, 3891−3893.
(5) Gao, Y. F.; Luo, H. J.; Zhang, Z. T.; Kang, L. T.; Chen, Z.; Du, J.; Kanehira, M.; Cao, C. X. *Nano Energy* **2012**, *1*, 221−246.
(6) Ni, J.; Jiang, W. T.; Yu, K.; Gao, Y. F.; Zhu, Z. Q. *Electrochim. Acta* **2011**, *56*, 2122−2126.
(7) Niu, C. J.; Meng, J. S.; Han, C. H.; Zhao, K. N.; Yan, M. Y.; Mai, L. Q. *Nano Lett.* **2014**, *14*, 2873−2878.
(8) Li, M.; Wu, X.; Li, L.; Wang, Y. X.; Li, D. B.; Pan, J.; Li, S. J.; Sun, L. T.; Li, G. H. *J. Mater. Chem. A* **2014**, *2*, 4520−4523.
(9) Peng, Z. F.; Jiang, W.; Liu, H. *J. Phys. Chem. C* **2007**, *111*, 1119−1122.
(10) Qi, J.; Ning, G. L.; Lin, Y. *Mater. Res. Bull.* **2008**, *43*, 2300−2307.
(11) Son, J.-H.; Wei, J.; Cobden, D.; Cao, G. Z.; Xia, Y. N. *Chem. Mater.* **2010**, *22*, 3043−3050.
(12) Gao, Y. F.; Cao, C. X.; Dai, L.; Luo, H. J.; Kanehira, M.; Ding, Y.; Wang, Z. L. *Energy Environ. Sci.* **2012**, *5*, 8708−8715.
(13) Li, Y. M.; Ji, S. D.; Gao, Y. F.; Luo, H. J.; Jin, P. *ACS Appl. Mater. Interfaces* **2013**, *5*, 6603−6614.
(14) Li, D. B.; Li, M.; Pan, J.; Luo, Y. Y.; Wu, H.; Zhang, Y. X.; Li, G. H. *ACS Appl. Mater. Interfaces* **2014**, *6*, 6555−6561.
(15) Rama, N.; Ramachandra Rao, M. S. *Solid State Commun.* **2010**, *150*, 1041−1044.
(16) Jian, J.; Wang, X. J.; Li, L. G.; Fan, M.; Zhang, W. R.; Huang, J. J.; Qi, Z. M.; Wang, H. Y. *ACS Appl. Mater. Interfaces* **2017**, *9*, 5319−5327.
(17) Wu, C. Z.; Dai, J.; Zhang, X. D.; Yang, J. L.; Qi, F.; Gao, C.; Xie, Y. *Angew. Chem., Int. Ed.* **2010**, *49*, 134−137.
(18) Jiang, B. J.; Peng, X.; Qu, Y.; Wang, H.; Tian, C. G.; Pan, Q. J.; Li, M. X.; Zhou, W.; Fu, H. G. *ChemCatChem* **2014**, *6*, 2553−2559.
(19) Wang, Y. T.; Chen, C. H. *Inorg. Chem.* **2013**, *52*, 2550−2555.
(20) Zhong, L.; Li, M.; Wang, H.; Luo, Y. Y.; Pan, J.; Li, G. H. *CrystEngComm* **2015**, *17*, 5614−5619.
(21) Zhu, J. T.; Zhou, Y. J.; Wang, B. B.; Zheng, J. Y.; Ji, S. D.; Yao, H. L.; Luo, H. J.; Jin, P. *ACS Appl. Mater. Interfaces* **2015**, *7*, 27796−27803.
(22) Zhang, L. M.; Xia, F.; Song, Z. D.; Webster, N. A. S.; Song, J. C.; Luo, H. J.; Gao, Y. F. *Inorg. Chem. Front.* **2016**, *3*, 117−124.
(23) Avansi, W., Jr.; Ribeiro, C.; Leite, E. R.; Mastelaro, V. R. *Cryst. Growth Des.* **2009**, *9*, 3626−3631.
(24) Corr, S. A.; Grossman, M.; Shi, Y. F.; Heier, K. R.; Stucky, G. D.; Seshadri, R. *J. Mater. Chem.* **2009**, *19*, 4362−4367.
(25) Zhang, Y. F.; Fan, M. J.; Liu, X. H.; Xie, G. Y.; Li, H. B.; Huang, C. *Solid State Commun.* **2012**, *152*, 253−256.
(26) Li, M.; Li, D. B.; Pan, J.; Lin, J. C.; Li, G. H. *Eur. J. Inorg. Chem.* **2013**, *2013*, 1207−1212.
(27) Yu, W. L.; Li, S.; Huang, C. *RSC Adv.* **2016**, *6*, 7113−7120.
(28) Li, N.; Huang, W. X.; Shi, Q. W.; Zhang, Y. B.; Song, L. W. *Ceram. Int.* **2013**, *39*, 6199−6206.
(29) Zhang, S. D.; Li, Y. M.; Wu, C. Z.; Zheng, F.; Xie, Y. *J. Phys. Chem. C* **2009**, *113*, 15058−15067.
(30) Shi, S. F.; Cao, M. H.; He, X.; Xie, H. M. *Cryst. Growth Des.* **2007**, *7*, 1893−1897.
(31) Zhang, Y. F.; Fan, M. J.; Liu, X. H.; Xie, G. Y.; Li, H. B.; Huang, C. *Solid State Commun.* **2012**, *152*, 253−256.
(32) Shi, S. F.; Cao, M. H.; He, X.; Xie, H. M. *Cryst. Growth Des.* **2007**, *7*, 1893−1897.
(33) Liu, L.; Cao, F.; Yao, T.; Xu, Y.; Zhou, M.; Qu, B. Y.; Pan, B.; Wu, C. Z.; Wei, S. Q.; Xie, Y. *New J. Chem.* **2012**, *36*, 619−625.
(34) Sun, X. M.; Chen, X.; Deng, Z. X.; Li, Y. D. *Mater. Chem. Phys.* **2003**, *78*, 99−104.
(35) Fan, W. L.; Song, X. Y.; Bu, Y. X.; Sun, S. X.; Zhao, X. *J. Phys. Chem. B* **2006**, *110*, 23247−23254.
(36) Gao, P.; Ying, C.; Wang, S. Q.; Ye, L. N.; Guo, Q.; Xie, Y. *J. Nanopart. Res.* **2006**, *8*, 131−136.
(37) Dai, L.; Cao, C. X.; Gao, Y. F.; Luo, H. J. *Sol. Energy Mater. Sol. Cells* **2011**, *95*, 712−715.
(38) Smrcok, L.; Bitschnau, B.; Filinchuk, Y. *Cryst. Res. Technol.* **2009**, *44*, 978−984.
(39) Park, H. K.; Kim, G. *Solid State Ionics* **2010**, *181*, 311−314.
(40) Chernova, N. A.; Roppolo, M.; Dillon, A. C.; Whittingham, M. S. *J. Mater. Chem.* **2009**, *19*, 2526−2552.
(41) Liu, J. F.; Li, Q. H.; Wang, T. H.; Yu, D. P.; Li, Y. D. *Angew. Chem., Int. Ed.* **2004**, *43*, 5048−5052.
(42) Wu, C. Z.; Zhang, X. d.; Dai, J.; Yang, J. L.; Wu, Z. Y.; Wei, S. Q.; Xie, Y. *J. Mater. Chem.* **2011**, *21*, 4509−4517.
(43) Lopez, R.; Haynes, T. E.; Boatner, L. A.; Feldman, L. C.; Haglund, R. F. *Phys. Rev. B: Condens. Matter Mater. Phys.* **2002**, *65*, 224113.
(44) Lopez, R.; Feldman, L.; Haglund, R. *Phys. Rev. Lett.* **2004**, *93*, 177403.
(45) Li, S. Y.; Niklasson, G. A.; Granqvist, C. G. *J. Appl. Phys.* **2010**, *108*, 063525.
(46) Zhong, L.; Luo, Y. Y.; Li, M.; Han, Y. Y.; Wang, H.; Xu, S.; Li, G. H. *CrystEngComm* **2016**, *18*, 7140−7146.
(47) Mlyuka, N. R.; Niklasson, G. A.; Granqvist, C. G. *Sol. Energy Mater. Sol. Cells* **2009**, *93*, 1685−1687.

DOI: 10.1021/acs.cgd.7b01037
Cryst. Growth Des. 2017, 17, 5927−5934